JOURNAL OF SYNCHROTRON RADIATION
ISSN 1600-5775

# Novel silica stabilization method for the analysis of fine nanocrystals using coherent X-ray diffraction imaging

Marianne Monteforte,[a]* Ana K. Estandarte,[a] Bo Chen,[a] Ross Harder,[b] Michael H. Huang[c] and Ian K. Robinson[a]

[a]London Centre for Nanotechnology, University College London, Gower Street, London WC1E 6BT, UK, [b]Argonne National Laboratory, Advanced Photon Source, Argonne, IL 60439, USA, and [c]National Tsing Hua University, Guangfu Rd, East District, Hsinchu City 300, Taiwan. *Correspondence e-mail: marianne.monteforte.10@ucl.ac.uk

Received 14 December 2015
Accepted 15 April 2016

Edited by G. Grübel, HASYLAB at DESY, Germany

**Keywords:** Bragg coherent X-ray diffraction; nanocrystals; stabilization method; three-dimensional reconstruction; strain.

High-energy X-ray Bragg coherent diffraction imaging (BCDI) is a well established synchrotron-based technique used to quantitatively reconstruct the three-dimensional morphology and strain distribution in nanocrystals. The BCDI technique has become a powerful analytical tool for quantitative investigations of nanocrystals, nanotubes, nanorods and more recently biological systems. BCDI has however typically failed for fine nanocrystals in sub-100 nm size regimes – a size routinely achievable by chemical synthesis – despite the spatial resolution of the BCDI technique being 20–30 nm. The limitations of this technique arise from the movement of nanocrystals under illumination by the highly coherent beam, which prevents full diffraction data sets from being acquired. A solution is provided here to overcome this problem and extend the size limit of the BCDI technique, through the design of a novel stabilization method by embedding the fine nanocrystals into a silica matrix. Chemically synthesized FePt nanocrystals of maximum dimension 20 nm and AuPd nanocrystals in the size range 60–65 nm were investigated with BCDI measurement at beamline 34-ID-C of the APS, Argonne National Laboratory. Novel experimental methodologies to elucidate the presence of strain in fine nanocrystals are a necessary pre-requisite in order to better understand strain profiles in engineered nanocrystals for novel device development.

## 1. Introduction

BCDI has been extensively developed by Ian K. Robinson over the last 20 years and requires highly coherent X-rays, generated by second- and third-generation synchrotron sources, to achieve a high spatial resolution (Robinson & Harder, 2009). In a typical BCDI experiment a coherent beam of X-rays illuminates the sample of nanocrystals from which three-dimensional diffraction data sets are collected from the Bragg peaks of isolated nanocrystals. This is achieved by rotating the sample through the Bragg condition in small increments to acquire a rocking-curve series. The diffraction data sets are then reconstructed using phase retrieval algorithms (Fienup, 1982) to achieve quantitative three-dimensional reconstructions of the nanocrystal morphology and strain distribution.

The radiation pressure of the focused coherent beam is expected to dominate the otherwise mostly van der Waals interaction between fine nanocrystals and the substrate. This undesired effect of the highly coherent X-ray beam results in movement of the nanocrystals, preventing full diffraction data sets (necessary for achieving good reconstructions) from being obtained. The limitations of the BCDI technique as a result of

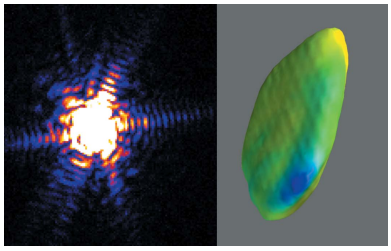

the highly coherent beam have also been identified in other BCDI investigations: Liang *et al.* (2014) detected the rotational single motion of nanocrystals in a viscoelastic colloidal gel matrix and Shi *et al.* (2012) observed radiation-induced bending of silicon nanowires.

In previous BCDI studies of un-bound nanocrystals with dimensions above 100 nm, the Bragg peak from an isolated nanocrystal was typically constant in position over time. This increased stability of the nanocrystal, derived from its larger dimensions of the nanocrystal, allowed full diffraction data sets to be obtained from the whole rocking-curve series. However, for BCDI studies of fine (sub-100 nm) un-bound nanocrystals, the Bragg peaks observed from the nanocrystals are not constant in position over time as a result of the inherent instability of the nanocrystals under illumination by the coherent beam. This instability of the nanocrystals was also observed in our previous BCDI investigations, performed at beamline 34-ID-C (of the Advanced Photon Source, Argonne National Laboratory), of fine un-bound FePt nanocrystals of maximum dimension 20 nm (Fig. 1). During the investigations, the movement of the nanocrystals resulted in streaks that resemble powder rings, preventing full diffraction data sets from being recorded. Additionally, the Bragg peaks from the nanocrystals appeared and disappeared within the 5 s exposure time of the detector as shown in Fig. 1(*a*), with peak visible, and Fig. 1(*b*) with no peak visible.

The instability of the fine FePt nanocrystals led to the motivation behind this study: to devise an efficient stabilization method to fix and effectively prevent the movement of fine nanocrystals during BCDI investigations. Prior to this investigation, two BCDI stabilization materials were tested to evaluate their efficacy in fixing the nanocrystals into a thin 'transparent' solid matrix: epoxy glue, which solidified at room temperature, and gallium indium, which solidified at its eutectic temperature on cooling *in situ*. The results of these studies revealed that both matrix materials displayed no indication of stabilization during the BCDI studies, and the nanocrystals remained unstable on illumination by the beam.

In this study, we investigate the use of silica as an effective matrix material. In addition to its amorphous nature and compatibility with the silicon substrate, silica has also been shown to successfully prevent nanocrystals from sintering during high-temperature heat treatments. Various stabilization methods already exist to coat nanocrystals with silica, creating a thermal protection barrier. These include (i) mechanical methods such as the use of nano-reactors (Chen *et al.*, 2010) and atomic layer deposition techniques (Liang *et al.*, 2010) and (ii) chemical methods such as modified Stöber coating (Chen *et al.*, 2011), and water and oil-in-water emulsion coating (Fan *et al.*, 2004). The mechanical methods, however, require access to instrumental coating equipment, which is not readily available at synchrotron facilities, and chemical coating methods

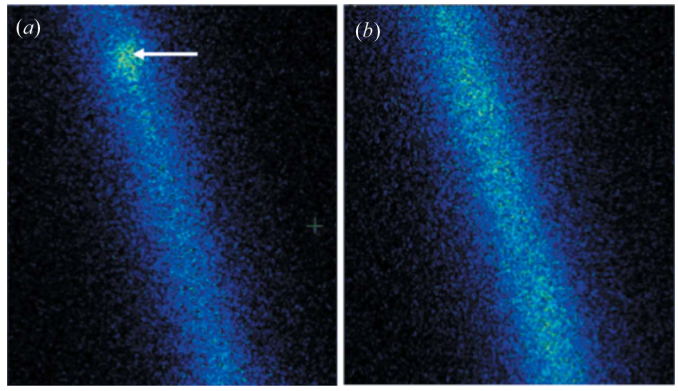


**Figure 1**
Diffraction frames from BCDI investigations of un-bound FePt nanocrystals on the FePt (111) diffraction plane with (*a*) Bragg peak appearing as indicated by the arrow and (*b*) with Bragg peak disappearing after 5 s exposure.

are typically complex and laborious (with reaction times of up to 24 h). In addition, current silica coating methods typically involve coating the nanocrystal surface to create a silica shell without describing the encapsulation of nanocrystals within a silica matrix on a substrate. In this study, we report on the development of a novel and prompt one-step silica-coating method based on the concept of sol–gel polymerization of tetraethyl orthosilicate (TEOS), in the presence of ethanol (Lu *et al.*, 2002), to create silica nanocomposites encapsulating the following chemically synthesized nanocrystals: FePt octapod nanocrystals of maximum dimension 20 nm and AuPd nanocrystals of dimensions 60–65 nm.

## 2. Materials and methods

### 2.1. Nanocrystal samples

FePt octapod nanocrystals [as shown in Fig. 2(*a*)], of maximum dimension 20 nm (stabilized with hydrophilic oleic acid and olelyamine surfactant layer), were fabricated following a thermal decomposition synthetic scheme.

AuPd nanocrystals [as shown in Figs. 2(*b*) and 2(*c*)] of dimensions 60–65 nm [stabilized with hydrophilic cetyltrimethylammonium bromide (CTAB) surfactant layer] were fabricated from chemical synthesis (Chiu *et al.*, 2014). The FePt nanocrystals were dispersed as a colloid in a nonpolar

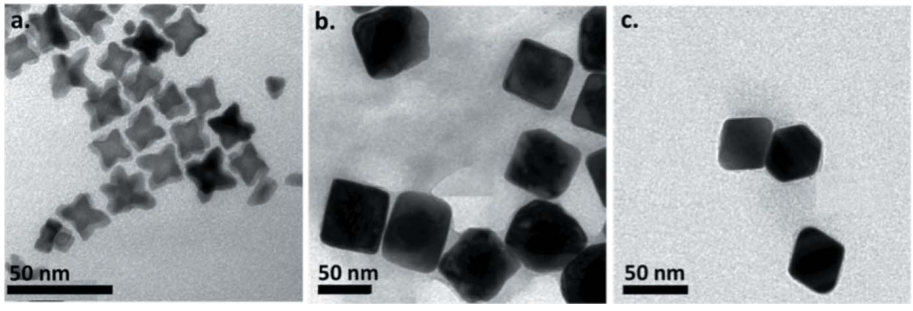


**Figure 2**
TEM images of FePt octapods (*a*) and AuPd nanocrystals from samples 1 (*b*) and 2 (*c*).

hexane suspension and the AuPd nanocrystal samples were dispersed as a colloid in a polar ethanol suspension.

### 2.2. Silica stabilization method

**2.2.1. Materials**. The following reagents used in the investigation were supplied by Sigma-Aldrich Ltd, UK, and are detailed as the following in their Materials Safety Data Sheets: tetraethyl orthosilicate (TEOS), $Si(OC_2H_5)_4$; 99.0% (GC), $M_w$ = 208.33 g mol$^{-1}$, purity = 98% (CP), $\rho$ = 0.993 g ml$^{-1}$ at 20°C, b.p. = 168°C; and ethanol (EtOH), $C_2H_5O$; 97% (GC), $\rho$ = 1.59 g ml$^{-1}$, b.p. = 78°C.

**2.2.2. TEOS solution drop-casting procedure**. The nanocrystals were embedded in a silica matrix through a 'drop-cast' stabilization method devised from the concept of sol–gel polymerization of tetraorthoxysilanes. On the basis that TEOS undergoes a hydrolysis–condensation reaction in the presence of EtOH and water, in this study a stock solution of TEOS and EtOH was devised (and it was assumed that water was absorbed from moisture in the air). The nanocrystal suspension was drop-cast onto a silicon substrate, forming a dry nanocrystal colloid on evaporation. Subsequently, the stock solution was drop-cast onto the dry colloid in ~20 µL drops, three times. During the drop-casting steps the substrate was maintained on a hot plate (at ~70°C) to encourage solvent evaporation.

**2.2.3. Sample annealing procedure**. The coated samples were annealed in an oven at specific temperatures and annealing times to promote polymerization and encourage a rigid silica network formation. The following annealing temperatures and times were investigated for the treatment of (*a*) FePt silica nanocomposite samples: 350°C for 4 h, 500°C for 4 h and 800°C for 90 min; and (*b*) AuPd silica nanocomposite samples: 350°C for 4 h and 600°C for 4 h. Through annealing, the samples changed from transparent to a slightly opaque white colour, which suggests the formation of a polymerized silica matrix.

**2.2.4. TEOS stabilization solution study**. Different silica matrix thicknesses were investigated with preliminary BCDI studies. The following concentration ratios of the stock solution, (TEOS):(EtOH), were investigated: 0.02:6 ml for stock solution 1, 0.04:6 ml for stock solution 2 and 0.07:6 ml for stock solution 3. The results of the study revealed that stock solutions 1 and 2 both provided a silica matrix that enabled encapsulation of the nanocrystals whilst remaining 'transparent' to the X-ray beam during alignment and measurements.

### 2.3. Instrumentation: beamline 34-ID-C set-up

The BCDI experiments were performed at the beamline 34-ID-C of the Advanced Photon Source, Argonne National Laboratory, whose instrumental set-up is described. A monochromatic X-ray beam was selected by adjusting the size of the undulator gap to tune the wavelength to 0.138 nm (giving an energy of approximately 9 keV). A pair of slits, placed before the focusing mirrors, is used to select a coherent beam with a size of 50 × 100 µm in the horizontal and vertical directions, respectively. Kirkpatrick–Baez mirrors were used to concentrate and focus the beam to 1 × 1 µm, maximizing the illuminating flux. Notably the focus needs to be larger than the nanocrystal for the BCDI technique to work. The X-ray beam was illuminated on the sample, positioned downstream. The diffracted beam passed an evacuated flight path of length 1.2–1.6 m to the Pilatus 100K detector (from Dectris, with 487 × 195 pixels and a pixel size of 172 × 172 µm) positioned on a robot arm. The detector angle was positioned to reach known powder rings at a $2\theta$ angle of (*a*) 36.35° to detect the FePt face-centred cubic (f.c.c.) (111) powder ring, (*b*) 29.31° to detect the FePt face-centred tetragonal (f.c.t.) (110) powder ring and (*c*) 34.22° to detect the AuPd f.c.c. (111) powder ring. Two-dimensional diffraction patterns were collected from isolated Bragg peaks of individual nanocrystals by rotating the sample through the Bragg condition in small increments (typically 0.002–0.01°). At each increment, another diffraction pattern was collected to acquire a full rocking-curve series surrounding the Bragg peak. Subsequently, the two-dimensional diffraction pattern data sets were collated to give a complete three-dimensional diffraction pattern set for reconstruction.

### 2.4. Reconstruction of nanocrystals

Rocking-curve scans of the desired nanocrystals were obtained by recording the diffraction patterns of the nanocrystals over an angular range around the Bragg peaks of the nanocrystals. The range of the rocking-curve scans was usually less than half a degree whereas the step size used was typically 0.005°. For the reconstruction procedure, the two-dimensional diffraction patterns making up the rocking curve of a measured crystal were stacked into one image using the *ImageJ* software. The resulting image had a total number of frames equivalent to the number of steps used in the rocking-curve scan of the crystal. The number of frames defined the size of the array in the *z*-axis. During the recording of the diffraction patterns, the full detector array was used and, hence, diffraction patterns from neighbouring nanocrystals could also be recorded. To remove unnecessary data and speed-up the reconstruction process, all of the frames in the stacked image were cropped to select only the diffraction pattern of interest. Other diffraction patterns present in the cropped image were removed to ensure that the cropped image contained only the diffraction pattern of interest. No binning was performed on the data.

After the data preparation, the phasing algorithm was performed on the measured diffraction pattern using MATLAB R2013a. The phasing algorithm involved iterative switching between real and Fourier space through the use of fast Fourier transform until known constraints in each domain had been satisfied. A random start was used as an initial guess of the object. The magnitude of the measured diffraction pattern was used as the Fourier space constraint while a support, inside which the electron density of the object was allowed to exist, was used as the real space constraint. The dimensions of the support were set according to the array size

of the diffraction pattern (and sample size) to give an oversampling ratio greater than two for each dimension. The main phasing algorithm used was guided-HIO (Chen *et al.*, 2007). The algorithm consisted of eight populations of random starts, all of which were subjected to 200 iterations of a combination of ER and HIO algorithms (Fienup, 1982). For the first five iterations, the ER algorithm was used. The algorithm was then switched to HIO. HIO was used until the 180th iteration, after which the algorithm was switched back to ER. A feedback parameter of 0.9 was used for the HIO algorithm. After the eight independent runs of the ER and HIO algorithms, the solution with the minimum error was selected and was used as a template for the next generation of eight independent runs of the ER and HIO algorithms. The template was used to generate the new set of guesses for the next generation, which was carried out by taking the geometric average of the template and the remaining seven solutions. Five generations of eight independent runs of ER and HIO algorithms were completed in total. During the ER and HIO iterations, the Shrinkwrap algorithm (Marchesini, 2007) was used to update the support as the iterations proceeded. This allowed a more accurate support of the object. The support was updated every five iterations by applying a Gaussian function to blur the current real-space estimate of the object and applying a threshold to the blurred image. Pixels with intensities below the threshold were excluded from the support. After the five generations of the ER and HIO algorithms, the average of the five best solutions was used as the final solution. The final solution obtained contains the real-space amplitude and phase of the crystal representing the Bragg electron density of the crystal and strain within the crystal, respectively. The software *ParaView* was used to generate the three-dimensional images of the reconstructed nanocrystals.

## 3. Results

### 3.1. BCDI stabilization investigation of FePt octapods and AuPd nanocrystals

In the BCDI investigations of the FePt–silica nanocomposite samples, annealed at 350°C for 4 h and 500°C for 4 h, observations of the FePt nanocrystals on the FePt (111) diffraction plane revealed very diffuse undefined Bragg peaks, as shown in the two different central Bragg diffraction frames in Figs. 3(*a*) and 3(*b*), respectively. These observed Bragg peaks were not constant in position over time, and it was concluded that the nanocrystals were unstable and were moving at such a rate that it was not possible to record a full rocking-curve series.

Only on rapid thermal annealing of the FePt–silica nanocomposite samples, annealed at 800°C for 90 min, was it possible to record a full rocking-curve series of an individual nanocrystal. Observations of the FePt nanocrystals on the FePt (111) diffraction plane revealed strongly saturated Bragg peaks with fine interference fringes as shown in the central Bragg diffraction frame in Fig. 4(*a*). The corresponding three-dimensional reconstruction in Fig. 4(*b*) reveals the morphology and strain distribution of the elongated FePt nanocrystal with dimensions $x$ = 151 nm, $y$ = 91 nm and $z$ = 76 nm. The colour scale in the strain distribution maps of the nanocrystal isosurface shows the relative phase shift (normalized to units in radians) in the range [−1.57, 1.57]. From observation of the strain distribution map of the FePt nanocrystal isosurface in Fig. 4(*b*), a region of strain can be seen at the lower edge (blue) that could be due to the redistribution and homogenous segregation of Fe or Pt during the larger crystal formation and phase transformation. The dimensions did not correspond well with the 20 nm dimensions of the original FePt specimen (obtained from TEM imaging), which indicates the crystallization of the fine nanocrystals to form a larger FePt nanocrystal. In addition, on further observation of the FePt nanocrystals the f.c.t. (110) diffraction plane was detected indicating a phase transformation of the FePt nanocrystals from the f.c.c. to f.c.t. phase (which typically occurs at temperatures above 400°C).

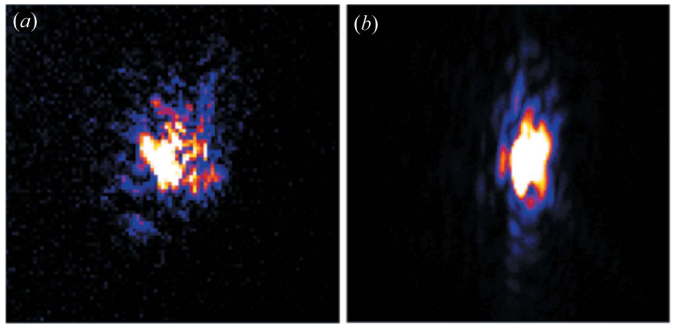


**Figure 3**
BCDI study of the FePt nanocrystals on the (111) diffraction in a FePt–silica nanocomposite (*a*) annealed at 350°C for 4 h and (*b*) annealed at 500°C for 4 h.

The FePt nanocrystal reconstruction is larger than the individual FePt octapods in the corresponding TEM image and is the result of the isolated FePt nanocrystals agglomerating during the rapid high-temperature annealing process. It is possible that instead of forming an encapsulating silica network (that would effectively isolate the FePt nanocrystals) the silica matrix only formed an 'over-layer' on the nanocrystals. Aslam *et al.* (2005) also observed this effect — resulting in an edgy partial coating of silica on the FePt nanocrystals — as a result of the surrounding hydrophilic oleic acid monolayer. Therefore, the oleic acid and oleylamine surfactant coating is not a compatible primer for silica and likely prevented the silica matrix encapsulation causing crystallization of the nanocrystals at high temperatures.

In the BCDI investigations of two AuPd silica nanocomposite samples, both annealed at 350°C for 4 h, observations of the AuPd nanocrystals on the AuPd (111) diffraction plane revealed intense Bragg peaks with a few diffraction fringes as shown in Figs. 4(*c*) and 4(*e*). The corresponding three-dimensional reconstruction [to Fig. 4(*c*)] is shown in Fig. 4(*d*) and reveals the morphology and strain distribution of the AuPd nanocrystals of dimensions $x$ = 113 nm, $y$ = 88 nm and $z$ = 94 nm. The morphology of the AuPd nanocrystal is

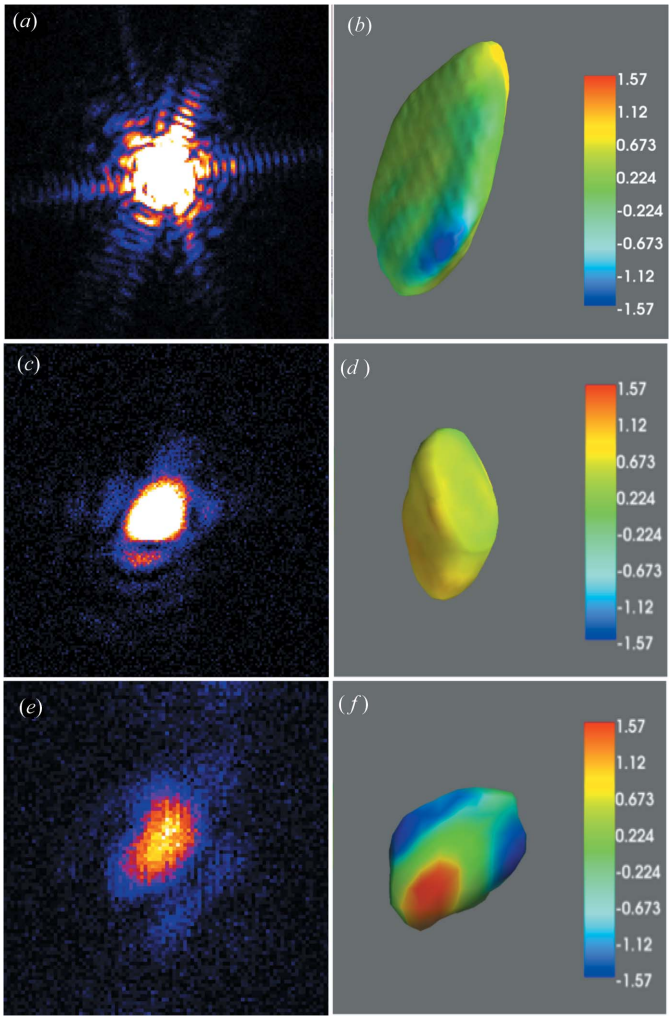


**Figure 4**
BCDI study of the (111) diffraction of nanocrystals in the FePt and AuPd silica nanocomposites. (*a*) Central Bragg diffraction frame of the FePt nanocrystal (annealed at 850°C for 90 min), (*b*) corresponding three-dimensional reconstruction of the FePt nanocrystal with morphology (151 × 91 × 76 nm) and strain isosurface (colour scale units in radians), (*c*) central Bragg diffraction frame of AuPd nanocrystal (sample 1 annealed at 350°C for 4 h), (*d*) corresponding three-dimensional reconstruction of AuPd nanocrystal with morphology (113 × 94 × 81 nm) and strain isosurface (colour scale units in radians), (*e*) central Bragg diffraction frame of AuPd nanocrystal (sample 2 annealed 350°C for 4 h) and (*f*) corresponding three-dimensional reconstruction of AuPd nanocrystal with morphology (62 × 56 × 62 nm) and strain isosurface (the colour scale in the strain distribution maps of the nanocrystal isosurface shows the relative phase shift, normalized to units in radians, in the range [−1.57, 1.57]).

slightly elongated with an ovoid shape and the strain isosurface shows a homogenous strain distribution.

The corresponding three-dimensional reconstruction [to Fig. 4(*e*)] is shown in Fig. 4(*f*) revealing the morphology and strain distribution of the AuPd nanocrystal of dimensions $x$ = 62 nm, $y$ = 56 nm and $z$ = 62 nm. The morphology of the AuPd nanocrystal is slightly ovoid and the strain isosurface indicates highly strained regions at its opposite edges. The reconstructions of the AuPd nanocrystals correspond reasonably with the dimensions obtained from TEM images, although for sample 1 are slightly larger which could be a result of agglomeration but could also be within the error of the reconstruction size measurements. Nevertheless, the high stability of the AuPd nanocrystals upon exposure to the beam suggests that the silica encapsulated the nanocrystal whilst also bonding to the substrate to create a rigid three-dimensional silica network.

## 4. Discussion

The results reveal a preferential stabilization of AuPd nanocrystals in comparison with the FePt nanocrystals, which could be the result of the larger initial size of the AuPd nanocrystals, and also a result of the different surfactant coatings. The functional group of the hydrophilic CTAB surfactant on the AuPd nanocrystal surface is compatible with the silica matrix and it is expected that the surfactant acts as a template encapsulating the nanocrystals in the silica matrix and the silicon substrate. During annealing, on reaching temperatures above the surfactant boiling point, it is expected that the surfactants evaporate through the pores of the silica matrix resulting in the formation of a rigid silica network. Additionally, the low annealing temperature is expected to have contributed towards retaining the structural integrity and phase of the AuPd nanocrystals. Furthermore, it is proposed that, at the annealing temperature of 350°C, eutectic bonding of the Si(substrate)–Au(nanocrystals) may have occurred [as Si–Au has a eutectic temperature as low as 250°C (Hamidinezhad *et al.*, 2011)].

In future BCDI studies, surfactant exchange with compatible surfactants such as organosilanes will encourage silica stabilization of nanocrystals coated with incompatible surfactants. Aslam *et al.* (2005) conducted surfactant exchange to cap the FePt nanocrystals with an aminoproxosilane surfactant layer to generate a more homogenous silica coating on the nanocrystal surface. It is expected that the functional group of silane will act as a primer for condensation of TEOS on the nanoparticle surface and promote interfacial bonding between the nanocrystal and the silica matrix (Palma *et al.*, 2007); thus, enabling a more rigid encapsulation matrix formation. In contrast, surface functionalization and surfactant exchange may not be necessary at all for some nanocrystals; in the case of Fe oxides the dominant hydroxide terminated surface will act as a nucleation site for TEOS condensation and hydrolysation.

## 5. Conclusions

In this study we demonstrate the feasibility of the novel one-step 'drop-cast' stabilization method as a prompt and efficient approach to extend the accessible size regime of the BCDI technique. Fine chemically synthesized nanocrystals with sub-100 nm dimensions were stabilized and from BCDI measurements three-dimensional reconstructions of the nanocrystals were achieved.

The BCDI investigations of the FePt nanocrystals in the FePt–silica nanocomposite, annealed at 350°C and 500°C for

4 h, were unstable and did not enable three-dimensional diffraction data sets to be acquired. The BCDI investigations of the FePt–silica nanocomposites, annealed at 800°C for 90 min, enabled full three-dimensional reconstructions (of dimensions $x$ = 151 nm, $y$ = 91 nm and $z$ = 76 nm) through the collection of complete rocking-curve data. The movement of the FePt nanocrystals was significantly prevented using this stabilization technique; however, the incompatible hydrophilic surfactants resulted in the formation of larger nanocrystals during the heat treatment stage.

The BCDI investigations of the two AuPd nanocrystals in the silica nanocomposites, both annealed at 350°C for 4 h, enabled three-dimensional reconstruction of the two AuPd nanocrystals of dimensions $x$ = 113 nm, $y$ = 88 nm and $z$ = 94 nm, and $x$ = 62 nm, $y$ = 56 nm and $z$ = 62 nm. In both investigations of the AuPd nanocrystal samples the movement of the nanocrystals was significantly prevented by the stabilization process, enabling full three-dimensional reconstructions through the collection of complete rocking-curve data.

The agglomeration of the nanocrystals during the heat treatment stage revealed avenues for future exploration to optimize the stabilization technique. Firstly, surface functionalization of the nanocrystals with a compatible surfactant, prior to stabilization, could prevent agglomeration of the nanocrystals during annealing. Secondly, exposure of the nanocomposites to lower annealing temperatures could also prevent agglomeration.

Overall this BCDI study reveals the potential to probe smaller nanocrystals than previously achievable through the design of novel stabilization techniques. The stabilization approach detailed within this study can be readily implemented without the use of extensive chemical procedures or coating equipment. Despite issues with agglomeration during the high-temperature annealing process, the success of this technique can also be seen by its rapid adoption by other APS beamline users (results as yet unpublished). Furthering the knowledge and understanding of the fundamental properties of fine nanocrystals (of sub-100 nm dimensions) will enable key applications in medicine, nano-catalysis and information technologies.

## Acknowledgements

This work was sponsored by a studentship to MM from the Diamond Light Source, an EPSRC grant EP/I022562/1, Phase modulation technology for X-ray imaging, and an ERC Advanced Grant 227711, Exploration of strains in synthetic nanocrystals.

## References

Aslam, M., Fu, L., Li, S. & Dravid, V. (2005). *J. Colloid Interface Sci.* **290**, 444–449.
Chen, C.-C., Miao, J., Wang, C. W. & Lee, T. K. (2007). *Phys. Rev. B*, **76**, 064113.
Chen, G.-S., Chen, C.-N., Tseng, T.-T., Wei, M.-H., Hsieh, J. & Tseng, W. (2011). *J. Nanosci. Nanotechnol.* **11**, 90–97.
Chen, Z., Cui, Z.-M., Niu, F., Jiang, L. & Song, W.-G. (2010). *Chem. Commun.* **46**, 6524–6526.
Chiu, C. Y., Yang, M. Y., Lin, F. C., Huang, J. S. & Huang, M. H. (2014). *Nanoscale*, **6**, 7656–7665.
Fan, H., Yang, K., Boye, D., Sigmon, T., Malloy, K., Xu, H., López, G. & Brinker, J. (2004). *Science*, **304**, 567–571.
Fienup, J. (1982). *Appl. Opt.* **21**, 2758–2769.
Hamidinezhad, H., Wahab, Y., Othaman, Z. & Ismail, A. (2011). *Appl. Surf. Sci.* **257**, 9188–9192.
Liang, M., Harder, R. & Robinson, I. K. (2014). *IUCrJ*, **1**, 172–178.
Liang, X., Barrett, K., Jiang, Y.-B. & Weimer, A. (2010). *Appl. Mater. Interfaces*, **2**, 2248–2253.
Lu, Y., Yin, Y., Mayers, B. & Xia, Y. (2002). *Nano Lett.* **2**, 183–186.
Marchesini, S. (2007). *Rev. Sci. Instrum.* **78**, 011301.
Palma, R. D., Peeters, S., Van Bael, M., Van den Rul, H., Bonroy, K., Laureyn, W., Mullens, J., Borghs, G. & Maes, G. (2007). *Chem. Mater.* **19**, 1821–1831.
Robinson, I. & Harder, R. (2009). *Nat. Mater.* **8**, 291–298.
Shi, X., Xiong, G., Huang, X., Harder, R. & Robinson, I. (2012). *New J. Phys.* **14**, 063029.